

# State of Charge estimation of lithium-ion power battery based on online parameter identification method and BP neural network

Shuai Qin<sup>1,\*</sup>, Dongchen Qin<sup>1</sup>, Hongxia Wu<sup>1,\*</sup>, Tingting Wang<sup>1</sup>, Jiangyi Chen<sup>1</sup>, Peizhuo Wang<sup>1</sup>

<sup>1</sup> School of Mechanical and Power Engineering, Zhengzhou University, Zhengzhou 450001, China

\*E-mail: [18738172859@163.com](mailto:18738172859@163.com), [wu\\_hx@zzu.edu.cn](mailto:wu_hx@zzu.edu.cn)

Received: 18 September 2021 / Accepted: 18 October 2021 / Published: 6 December 2021

---

The accurate estimation of power battery state of charge (SOC) is of great significance to vehicle driving safety and energy management. In this paper, the second-order RC equivalent circuit model is used, the recursive least square method with forgetting factor (FFRLS) is used for online parameter identification, and the extended Kalman filter (EKF) is used for SOC estimation. The off-line data charging and discharging under each working condition of the battery are used as training data, the BP neural network is used for training, and the estimation error of the extended Kalman filter is used as the training output of the neural network to compensate for the error of the extended Kalman filter. FFRLS and EKF are used to ensure the real-time performance of the system, and FFRLS and BP neural networks are used to improve the robustness of the system. It is proven through simulation that this method can effectively improve the accuracy of SOC estimation.

---

**Keywords:** Online parameter identification; recursive least squares method; BP neural network; extended Kalman filter; robustness; real-time.

## 1. INTRODUCTION

The rapid development of the global economy also brings environmental and energy issues. The emission of carbon dioxide and harmful pollutants has become a focus of international attention. To reduce the consumption of fossil fuels by vehicles and alleviate energy resources and demands, the development of vehicles powered by novel energy sources has achieved global consensus. As the core energy storage unit for vehicles powered by new energy sources, power batteries directly impact performance. Lithium-ion batteries have become the leading energy unit product of new energy vehicles because of their high energy density, high power density, and long service life. The SOC of the battery has a significant influence on the driving performance of the vehicle. An accurate SOC can ensure the safe and reliable operation of the power battery and provide an adequate basis for vehicle

energy management and safety management. The research and optimization of battery SOC estimation have always represented a hot direction for many universities and enterprises[1,2].

The model-based SOC estimation method uses the model and state estimation calculation method to complete the estimation of the power battery SOC. This method first needs to establish a reliable model and state equation and apply filter algorithms and observers to estimate the SOC. The model-based approach is a closed-loop iterative process, which makes the algorithm robust to a certain extent by continuously revising the SOC estimation value. Generally, a model-based method includes three steps: model building, parameter estimation, and estimation algorithm. This article adopts a model-based SOC estimation method, and the development status of this method is sorted out below[6].

The model is built, and it is found through experiments that the output voltage of the power battery is accompanied by electrochemical polarization, which has strong time-variance and strong nonlinearity. To simulate the working state of the battery and guide engineering applications, it is necessary to build a model that can instantiate this reaction and elucidate the mathematical relationship between the various parameters based on the principles of physics and chemistry [3,7]. Standard power battery models are mainly electrochemical models, equivalent circuit models, and fractional-order batteries based on comparable circuit models and AC impedance characteristics[8,10].

For model parameter identification, the filtering process in the Kalman filter algorithm requires dynamic data such as current and terminal voltage collected by the sensor and other parameters in the model. These parameters are generally not directly available and need to be obtained using specific methods. The accuracy of the parameters will affect the accuracy of the SOC estimation. Parameter identification can be divided into offline parameter identification and online parameter identification based on real-time performance.

Online parameter identification calculates real-time measured current, voltage, temperature, and other parameters realizes online updating of parameters, ensures strong followability, achieves solid real-time performance, and does not require a large amount of offline experimental data. Xiang wei Guo uses the recursive least squares method with a forgetting factor and unscented Kalman filter to estimate the SOC to enhance the real-time performance. It is proven through simulation that the estimation accuracy is higher than that of a single unscented Kalman filter [24]. Rui Xiong uses the multiscale dual-extended Kalman filter, sets different online parameter identification and calculation frequencies of SOC estimation, effectively overcomes the problem of initial capacity change with the environment, improves SOC estimation accuracy while reducing calculation time, and increases estimation efficiency by 47%[25]. Rui Xiong used the least squares method as the online number estimation method, combined with the electrochemical polarization model, and the simulation proved that the error between the simulated terminal voltage and the experimental value was controlled within 1% [15]. According to the power battery discharge current, Cheng Zhang set different parameter update frequencies under different current frequencies to optimize the online parameter identification method. Simulations and experiments prove that this parameter identification method can improve the accuracy of SOC estimation [14]. H. Rahimi uses the moving window least squares method for parameter identification. This method can determine the length of the window according to the degree of fluctuation of the input data, which makes up for the shortcomings of the recursive least squares

method that relies on frequent data excitation to achieve accurate identification [17, 18]. The above are all based on the optimization algorithm of the extended Kalman filter or least square method for online parameter identification, but both algorithms have shortcomings. A double extended Kalman filter needs to select different estimation frequencies, and the least square process requires fluctuation. Even if online parameter recognition is used, frequent excitation can improve accuracy, but it still needs to be optimized.

SOC estimation is an essential aspect of electric vehicle battery management systems and is the basis for ensuring the safe operation of the power battery systems. The Kalman filtering algorithm is commonly utilized in power battery SOC estimation methods. It takes the estimator as a spatial state variable, makes full use of the measurable data in the battery system, and uses the recursive approach to filter out the design and random noise to obtain an accurate space state value[4,9]. M.Mastali compared the ampere-hour integration method, extended Kalman filter, and double extended Kalman filter method, taking the circular battery and square battery as the research object; through simulation analysis, the double extended Kalman filter was found to be more adapted to different types of batteries and to take real-time performance and accuracy into account[23]. Xiong Rui used dual Kalman filtering to estimate the SOC and equivalent circuit model parameters separately and used different update frequencies according to the change characteristics of the two variables to achieve improved accuracy and real-time performance of SOC estimation [25]. Xiangwu Yan used the GNL equivalent circuit model to consider the battery's self-discharge coefficient to reflect the battery's static and dynamic power changes more accurately. At the same time, the estimation accuracy of the EKF and AUKF methods is compared, and the simulation proves that the estimation effect of AUKF is better[26]. Hongwen He compared the estimation accuracy of the EKF and UKF. From the estimation accuracy and convergence speed as comparison parameters, simulations prove that UKF and EKF can effectively overcome the shortcomings of inaccurate initial SOC values, but the convergence speed and estimation accuracy of the UKF are better than those of the EKF [32]. Through the above analysis, Kalman filtering and derivative algorithms are shown to belong to the mainstream direction of SOC estimation, but Kalman filtering cannot meet the accuracy of the actual production requirements of SOC. Because of the linear approximation steps in the algorithm principle, there will be errors. When high accuracy is required, it is necessary to improve the model parameters and algorithm optimization to obtain better results.

Based on a data-driven method, this method is effective in dealing with nonlinear problems. The typical representative of this type of method is the neural network model, which does not need to consider the internal reaction mechanism of the power battery and can estimate the relevant parameters in the battery system. It has robust fitting ability and is suitable for any power battery. Mohammad use the RBF neural network model to estimate battery parameters. The voltage at the last moment, the current at that moment, and the SOC obtained by the ampere-hour integration method are used as the input of the NN, and the terminal voltage at this moment is used as the model output. In the EKF calculation using this terminal voltage, the simulation shows that better estimation accuracy can be attained[21]. Chang Cheng used the BP neural network model to estimate the SOH. Through analysis, the open-circuit voltage difference and the ohmic impedance of the battery were found to change according to the conditions of different cycles. The neural network was used to estimate the SOH, and

the estimation error was less than 5% [28]. Chao Dong used the momentum backpropagation algorithm to build a BP neural network model to estimate SOC, design a dynamic momentum factor to ensure the convergence speed, and prove through simulation that the SOC estimation can be accurate to within 4% [27]. Cheng Bo selects the parameters required for training according to the degree of correlation between the parameters and the SOC, uses a new immune evolution algorithm to optimize the weights in the BP neural network, and estimates the SOC through the optimized neural network, accuracy within 5% can be reached[30]. Bizhong Xia uses the Levenberg-Marquardt algorithm to optimize the weights of the wavelet transform of neural network and then uses the trained neural network to optimize the particle filter to obtain a more accurate SOC [33]. The neural network has strong learning ability. For the BP neural network, the weight optimization and learning data quality directly affect the training result during direction propagation.

Based on the above analysis and research, this paper proposes an SOC estimation method which uses an online parameter identification method to estimate model parameters, uses EKF to estimate SOC, and then uses a BP neural network to compensate for SOC estimation results to ensure accurate real-time estimation. Through simulation, it can be proven that the method proposed in this paper can effectively improve the estimation accuracy of SOC.

## 2. ESTABLISHMENT OF BATTERY MODEL

The battery model is used to describe the external characteristics of the battery during operation and reflect the changes in various parameters of the battery during charging and discharging. Because the battery's internal components are connected with DC impedance, the battery also undergoes polarization reaction due to the inner reaction mechanism during the charging and discharging process. The Thevenin model can reflectively the phenomenon of this battery[7]. Experiments show that the Thevenin model of the second-order RC network has better simulation efficiency. Consider the discharge data of the battery in a specific HPPC discharge experiment during the resting stage and the utilization of equations of different orders to fit the voltage and time. Referring to Figure 1, and with respect to the fitting results in Table 1 and consideration of the calculation efficiency, this paper adopts the Thevenin model of the second-order RC network. Figure 2 is a schematic diagram of the equivalent circuit model[5,16,22].

In Figure 2,  $U_{OC}$  is the open circuit voltage,  $U_L$  is the terminal voltage,  $I$  is the operating current,  $R_p$  and  $R_s$  are polarization resistances,  $C_p$  and  $C_s$  are polarization capacitances,  $R_0$  is ohmic internal resistance,  $U_p$  and  $U_s$  are polarization voltages, and  $U_0$  is the ohmic voltage across the internal resistance.

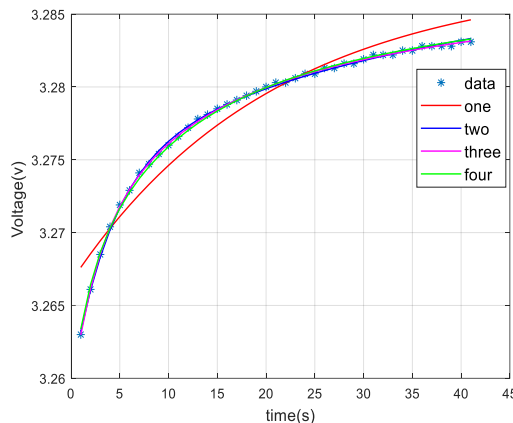


Figure 1. RC network fitting curves for order 1-4.

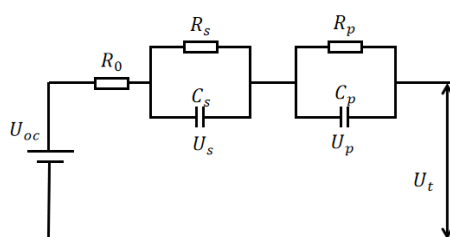


Figure 2 Second-order RC equivalent circuit model

Table 1. Fitting accuracy of each order equation

RC order	Error sum of squares	Standard deviation	Coefficient of determination
First order	6.368e-07	1.278e-3	0.8836
Second order	1.72e-06	2.156e-4	0.9969
Third order	4.43e-07	1.125e-4	0.9992
Fourth order	5.335e-06	4.021e-4	0.9885

From the physical relationship of the components in Figure 2 and according to Kirchhoff's law, we can obtain:

$$\dot{U}_p = \frac{I}{C_p} - \frac{U_p}{R_p C_p} \quad (1)$$

$$\dot{U}_s = \frac{I}{C_s} - \frac{U_s}{R_s C_s} \quad (2)$$

$$U_t = U_{OC} - U_p - U_s - IR \quad (3)$$

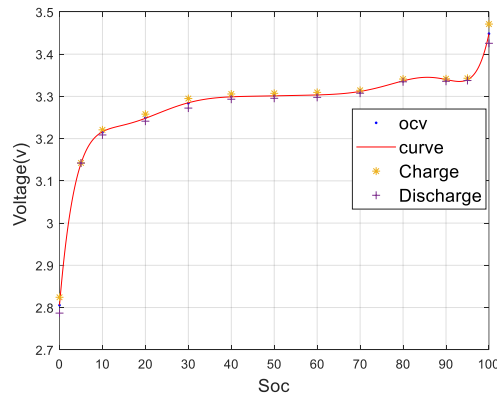


**Figure 3.** SOC-OCV battery curve

Experiments have proven that the open-circuit voltage and SOC have the same changing trend and exhibit a specific corresponding relationship with the SOC value [15]: that is, the OCV-SOC curve of the battery. Generally, different SOC values are obtained through hybrid plus power characteristic. The curve is obtained after fitting the open-circuit voltage below the SOC. Because the battery exhibits voltage hysteresis during charging and discharging, the voltage during charging is always higher than the voltage during discharge. This hysteresis effect is mainly attributed to the internal structure and working principle of lithium-ion batteries. This article takes the average value of the open-circuit voltage during charging and discharging and obtains the OCV-SOC curve shown in Figure 3 [7].

### 3. ONLINE PARAMETER RECOGNITION

The online parameter estimation method can improve the real-time performance and robustness of parameter estimation. This paper adopts the recursive least squares method (FFRLS) with the forgetting factor as parameter identification. The basic idea of the recursive least squares method is to add the last estimated value and the correction term to obtain a newly assessed value and overcome the model parameter uncertainty through typical parameter correction and updating. Increasing the forgetting factor reduces the previous weight. The information volume of data creates conditions for supplementing new data. The system equation of the battery is as follows:

$$y_k = \Phi_k \theta_k + e_k \tag{4}$$

$y_k$  is the output variable, which in this system is the instantaneous terminal voltage at the moment,  $\Phi_k$  is the observed variable in the system, which in the battery system is the matrix composed of the terminal voltage and current at the previous moment,  $\theta$  is the parameter matrix, the parameters in the battery system can be calculated through the parameters in the matrix and  $e_k$  is the stationary zero-mean white noise. The  $k$  in the lower right corner of each variable represents the  $k$  time.

The algorithm iteration process of the recursive least squares method with the forgetting factor is as follows:

$$K_k = P_k \Phi_k^T [\Phi_k P_{k-1} \Phi_k^T + \mu]^{-1} \tag{5}$$

$$\hat{\theta}_k = \hat{\theta}_{k-1} + K_k [y_k - \Phi_k \hat{\theta}_{k-1}] \quad (6)$$

$$P_k = \frac{1}{\mu} [I - K_k \Phi_k] P_{k-1} \quad (7)$$

$\mu$  is the forgetting factor,  $K_k$  is the algorithm gain, and  $P_k$  is the error covariance matrix of the parameter estimates. First, the algorithm gain is calculated and used along with the terminal voltage prediction error to determine the correction of the predicted value, and the error covariance matrix of the parameter estimates is ultimately updated until the algorithm end requirement is met.

To facilitate applying the FFRLS algorithm in the battery system, it is necessary to discretize the space state equation of the equivalent circuit model. According to the second-order identical circuit model and the physical relationship, it can be pulled-transformed and obtained in the frequency domain. The equation:

$$U_t(s) - U_{oc}(s) = -I(s) \left( R_0 + \frac{R_s}{1 + R_s C_s s} + \frac{R_p}{1 + R_p C_p s} \right) \quad (8)$$

Obtain the transfer function of the second-order model through (8).

$$G(s) = \frac{U_t(s) - U_{oc}(s)}{I(s)} = - \left( R_0 + \frac{R_s}{1 + R_s C_s s} + \frac{R_p}{1 + R_p C_p s} \right) \quad (9)$$

The bilinear transformation method is commonly used to map the system from the s-plane to the z-plane. In this paper, the method in (10) is used for the bilinear transformation.

$$s = \frac{2(1 - z^{-1})}{T(1 + z^{-1})} \quad (10)$$

T is the sampling frequency; in this article, T=1s. The equation based on the z-plane is:

$$G(z^{-1}) = \frac{c_3 + c_4 z^{-1} + c_5 z^{-2}}{1 - c_1 z^{-1} - c_2 z^{-2}} \quad (11)$$

Equation (11) can be transferred to the discrete time domain, and the result is:

$$U_{t,k} = (1 - c_1 - c_2)U_{oc} + c_1 U_{t,k-1} + c_2 U_{t,k-2} + c_3 I_k + c_4 I_{k-1} + c_5 I_{k-2} \quad (12)$$

According to system equation (4), formula (12) is transformed into the form of a matrix product:

$$\Phi(k) = [1 \quad U_{t,k-1} \quad U_{t,k-2} \quad I_k \quad I_{k-1} \quad I_{k-2}] \quad (13)$$

$$\theta(k) = [(1 - c_1 - c_2)U_{oc,k} \quad c_1 \quad c_2 \quad c_3 \quad c_4 \quad c_5]^T \quad (14)$$

Equation (13) is the observation variable matrix, and  $U_{t,k}$ ,  $U_{t,k-1}$ ,  $U_{t,k-2}$ ,  $I_k$ ,  $I_{k-1}$ , and  $I_{k-2}$  are the terminal voltage and current values at  $k$  time,  $k-1$  time, and  $k-2$  time, respectively.  $U_{oc,k}$  is the open circuit voltage at the  $k$  moment. Equation (14) is the parameter matrix.

The FFRLS algorithm needs to initialize some of the parameters during the calculation so that the error covariance matrix  $P_0 = \alpha I$ ,  $\alpha$  is as large as possible,  $I$  is the unit matrix, the forgetting factor  $\mu = 0.99$ , and  $\theta_0$  can take any value. Afterwards, iterative calculations are performed to obtain the parameter matrix, and then simple calculations are performed to obtain the battery system parameter values.

$$R_0 = \frac{-c_3 + c_4 - c_5}{1 + c_1 - c_2} \quad (15)$$

$$\tau_s = \frac{\left( -\sqrt{\frac{T^2(c_1^2 + 4c_2)}{(c_1 + c_2 - 1)^2}} - \frac{T(c_2 + 1)}{c_1 + c_2 - 1} \right)}{2} \tag{16}$$

$$\tau_p = \frac{\left( \sqrt{\frac{T^2(c_1^2 + 4c_2)}{(c_1 + c_2 - 1)^2}} - \frac{T(c_2 + 1)}{c_1 + c_2 - 1} \right)}{2} \tag{17}$$

$$R_s = \left( \begin{array}{c} \frac{\tau_1(c_1 - c_4 + c_5)}{c_1 - c_2 + 1} - \frac{T(c_3 - c_5)}{c_1 + c_2 - 1} + \frac{\tau_1(c_3 + c_4 + c_5)}{c_1 + c_2 - 1} \\ + \frac{T(c_2 + 1)(c_1 - c_4 + c_5)}{(c_1 + c_2 - 1)(c_1 - c_2 + 1)} \end{array} \right) (\tau_1 - \tau_2) \tag{18}$$

$$R_p = \frac{-c_3 - c_4 - c_5}{1 - c_1 - c_2} - R_0 - R_s \tag{19}$$

$$C_s = \frac{\tau_s}{R_s} \tag{20}$$

$$C_p = \frac{\tau_p}{R_p} \tag{21}$$

The obtained  $R_0, R_s, R_p, C_s, C_p$  are used as model parameters in the EKF algorithm to estimate the SOC[12,13,24].

## 4. SOC ESTIMATION

### 4.1 Extended Kalman Filter

The basic idea of the EKF algorithm is to expand the nonlinear equations of the system using the Taylor expansion formula and then use the KF algorithm to recursively achieve an approximate estimation of the state variables of the nonlinear system. The system state equation and system observation equation of the standard linear system are as follows:

$$x_k = A_k x_{k-1} + B_k u_k + w_k \tag{22}$$

$$y_k = C_k x_k + D_k u_k + v_k \tag{23}$$

General engineering application systems are mostly nonlinear systems. The following are the system state equations and system observation equations of the nonlinear system:

$$x_k = f(x_{k-1}, u_{k-1}) + w_{k-1} \tag{24}$$

$$y_k = h(x_k, u_k) + v_k \tag{25}$$

In equations (22),(23),(24) and (25) , $x_k$  are the state vectors, which are composed of the polarization voltage and SOC at time  $k$  in the battery system, the observation vector is  $y_k$ , which is the terminal voltage in the battery system at time  $k$ , and the white noise of the system is  $w_k$ , the measured white noise is  $v_k$ , the mean value of  $w_k$  and  $v_k$  is 0, and the covariance matrix is

represented by  $Q_k$  and  $R_k$  respectively.

Because the system that needs to participate in the Kalman filter algorithm calculation needs to be linear, the sum is Taylor expanded, the first-order term is retained, and the higher-order word is ignored to approximate the linearization of the nonlinear system as in: Equation (23) and Equation (24) is the approximate transformation equation.

$$f(x_k, u_k) \approx f(\hat{x}_k, u_k) + \left. \frac{\partial f(x_k, u_k)}{\partial x_k} \right|_{x=\hat{x}_k} (x_k - \hat{x}_k) \tag{26}$$

$$h(x_k, u_k) \approx h(\hat{x}_k, u_k) + \left. \frac{\partial h(x_k, u_k)}{\partial x_k} \right|_{x=\hat{x}_k} (x_k - \hat{x}_k) \tag{27}$$

Substituting Formulas (26) and (27) into Formulas (22) and (23), we obtain:

$$x_k \approx A_{k-1}x_{k-1} + \left[ f(\hat{x}_{k-1}, u_{k-1}) - A_{k-1}\hat{x}_{k-1} \right] + w_{k-1} \tag{28}$$

$$y_k \approx C_k x_k + \left[ h(\hat{x}_k, u_k) - C_k \hat{x}_k \right] + v_k \tag{29}$$

Define

$$A_k = \left. \frac{\partial f(x_k, u_k)}{\partial x_k} \right|_{x_k=\hat{x}_k}, \quad C_k = \left. \frac{\partial h(x_k, u_k)}{\partial x_k} \right|_{x_k=\hat{x}_k}, \quad B_k u_k = f(\hat{x}_{k-1}, u_{k-1}) - A_{k-1}\hat{x}_{k-1},$$

$$C_k u_k = h(\hat{x}_k, u_k) - C_k \hat{x}_k \tag{30}$$

The approximate linear transformation of the system equation has been completed, and the physical quantities of the battery system are substituted into the transformed nonlinear system. After discretizing the physical equations in the equivalent circuit model, the following state equations can be obtained.

$$SOC_k = SOC_{k-1} - \frac{\Delta t}{C_N I_{k-1}} \tag{31}$$

$$U_{s,k} = e^{\frac{-\Delta t}{R_s C_s}} U_{s,k-1} + \left( 1 - e^{\frac{-\Delta t}{R_s C_s}} \right) R_s I_{k-1} \tag{32}$$

$$U_{p,k} = e^{\frac{-\Delta t}{R_p C_p}} U_{p,k-1} + \left( 1 - e^{\frac{-\Delta t}{R_p C_p}} \right) R_p I_{k-1} \tag{33}$$

$$U_{t,k} = U_{oc}(SOC_k) - R_0 I_k - U_{s,k} - U_{p,k} + v_k \tag{34}$$

Convert the above formula into the form of a matrix.

$$\begin{bmatrix} U_{s,k} \\ U_{p,k} \\ SOC_k \end{bmatrix} = \begin{bmatrix} e^{\frac{-\Delta t}{R_s C_s}} & 0 & 0 \\ 0 & e^{\frac{-\Delta t}{R_p C_p}} & 0 \\ 0 & 0 & 1 \end{bmatrix} \begin{bmatrix} U_{s,k-1} \\ U_{p,k-1} \\ SOC_{k-1} \end{bmatrix} + \begin{bmatrix} R_s \left( 1 - e^{\frac{-\Delta t}{R_s C_s}} \right) \\ R_p \left( 1 - e^{\frac{-\Delta t}{R_p C_p}} \right) \\ -\frac{\Delta t}{C_n} \end{bmatrix} I_k \tag{35}$$

$$U_{t,k} = [-1 \quad -1 \quad \frac{\partial U_{oc,k}}{\partial SOC_k}] \begin{bmatrix} U_{s,k} \\ U_{p,k} \\ SOC_k \end{bmatrix} \tag{36}$$

Corresponding to the matrices in Equations (35) and (36) and the matrices in (22) and (23) in the linear system, the following matrices can be obtained.

$$\text{Transfer matrix } A_k = \begin{bmatrix} e^{\frac{-\Delta t}{R_s C_s}} & 0 & 0 \\ 0 & e^{\frac{-\Delta t}{R_p C_p}} & 0 \\ 0 & 0 & 1 \end{bmatrix}, \text{Feedforward matrix } D_k = R_0,$$

$$\text{Output matrix } C_k = \begin{bmatrix} -1 & -1 & \frac{\partial U_{oc}(SOC_k)}{\partial SOC_k} \end{bmatrix},$$

$$\text{Output matrix } B_k = \begin{bmatrix} R_s \left( 1 - e^{\frac{-\Delta t}{R_s C_s}} \right) & R_p \left( 1 - e^{\frac{-\Delta t}{R_p C_p}} \right) & \frac{-\Delta t}{C_n} \end{bmatrix}^T$$

After obtaining the system state equation and the observation state equation, some parameters in the EKF need to be initialized so that the initial matrix of the error covariance matrix  $P_0 = [0.0001 \quad 0.0001 \quad 1]^T I$ , the system noise error covariance matrix  $Q = \sigma I$ , and the  $\sigma$  value can take a relatively large number, EKF iteration may then proceed.

$$\hat{x}_k^- = f(\hat{x}_{k-1}, u_{k-1}) \tag{37}$$

$$P^- = A_k P_{k-1} A_k^T + Q_{k-1} \tag{38}$$

$$e_k = y_k - h(\hat{x}_k^-, u_k) \tag{39}$$

$$K_k = P_k^- C_k^T (C_k P_k^- C_k^T + R_{k-1})^{-1} \tag{40}$$

$$\hat{x}_k = \hat{x}_k^- + K_k e_k \tag{41}$$

$$P_k = (I - K_k C_k) P_k^- \tag{42}$$

In Formula (35),  $\hat{x}_k^-$  is the prior state value of the state vector,  $\hat{x}_k$  is the posterior state value of the state vector,  $P^-$  is the prior state error covariance matrix,  $P_k$  is the posterior state error covariance matrix, and  $e_k$  is the innovation. The EKF estimated SOC result is obtained through iteration[11,12,14,15,23].

## 4.2 BP neural network

### 4.2.1 The structure of the BP neural network

The BP neural network is also called the error backpropagation neural network. It is a feedforward network composed of nonlinear transformation units. It can learn and store a large amount of data without revealing the mathematical relationship between system variables in advance. The learning rule is to use a specific learning method to continuously adjust the weights and thresholds of

the network through backpropagation to minimize the sum of squared errors of the network to meet the target value. The topological structure of the BP neural network model includes the input layer, hidden layer, and output layer.

The input vector of the network is  $X = (x_1 \cdots x_i \cdots x_n)^T$ , the output vector of the hidden layer is  $Y = (y_1 \cdots y_j \cdots y_m)^T$ , the output layer vector represents  $O = (o_1 \cdots o_k \cdots o_l)^T$ , the expected output vector of the neural network is  $D = (d_1 \cdots d_k \cdots d_l)^T$ , the weight matrix from the input layer to the hidden layer is  $V = (v_1 \cdots v_j \cdots v_m)^T$ , and the weight matrix of the output layer is  $W = (w_1 \cdots w_k \cdots w_l)^T$ .

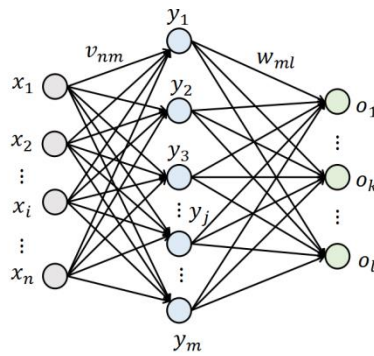


Figure 4. BP neural network structure

The mathematical expression of the output layer:

$$\begin{cases} o_k = f(\text{net}_k) & k = 1, 2, \dots, l \\ \text{net}_k = \sum_{j=1}^m w_{jk} y_j & k = 1, 2, \dots, l \end{cases} \quad (43)$$

The mathematical expression of the hidden layer:

$$\begin{cases} y_j = f(\text{net}_j) & j = 1, 2, \dots, m \\ \text{net}_j = \sum_{i=1}^n v_{ij} x_i & j = 1, 2, \dots, m \end{cases} \quad (44)$$

In Equations (36) and (37), the activation function generally uses unipolar sigmoid function:

$$f(x) = \frac{1}{1 + e^{-x}} \quad (45)$$

For the error and weight adjustment of the network, the error is defined as:

$$E = \frac{1}{2} (D - O)^2 = \frac{1}{2} \sum_{k=1}^l (d_k - o_k)^2 \quad (46)$$

Substituting Equations (43) and (44) into Equation (46), we can obtain:

$$E = \frac{1}{2} \sum_{k=1}^l \left\{ d_k - f \left[ \sum_{j=1}^m w_{jk} f \left( \text{net}_j \right) \right] \right\}^2 = \frac{1}{2} \sum_{k=1}^l \left\{ d_k - f \left[ \sum_{j=1}^m w_{jk} f \left( \sum_{i=1}^n v_{ij} x_i \right) \right] \right\}^2 \quad (47)$$

When the weight is adjusted, the BP neural network is adjusted according to the negative gradient direction, namely:

$$\begin{aligned} \Delta w_{jk} &= -\eta \frac{\partial E}{\partial w_{jk}} \quad j = 0, 1, 2, \dots, m \quad k = 1, 2, \dots, l \\ \Delta v_{ij} &= -\eta \frac{\partial E}{\partial v_{ij}} \quad i = 0, 1, 2, \dots, n \quad j = 1, 2, \dots, m \end{aligned} \tag{48}$$

It can be seen from the above formula that the estimation error of the network can be expressed as a correlation function composed of the hidden layer weight  $w_{jk}$  and the input layer weight  $v_{ij}$ . Adjusting the weight of the network can change the estimation error of the network. In the process of non-iterative calculation, the BP neural network continuously reduces the error by adjusting the weights and thresholds to meet the accuracy requirements.

The negative sign in Equation (48) indicates that the weight adjustment direction is the negative direction of the gradient, and  $\eta$  is the learning rate of the neural network, where a large learning rate will cause the system to be unstable, but a small learning rate will cause the convergence to be too slow and prolong the training time, the learning rate  $\eta$  of this article is 0.05. The second step is to determine the number of nodes in the hidden layer. Generally, empirical formulas are used to determine the number of nodes in the input layer,  $n$  is the number of nodes in the hidden layer,  $m$  is the number of nodes in the output layer, and  $l$  is a constant between 1-10. The number of nodes  $x$  of the hidden layer is determined by an empirical formula, as shown in the following formula.

$$x = \sqrt{n + m} + a \tag{49}$$

When the BP neural network preprocesses the data, it conducts polarity normalization processing. The purpose is to limit each sample variable to the interval of [0,1] or [-1,1], to ensure that each variable during training with equal weights, it can also avoid errors in network training caused by overloading of neurons to excessive input variable values. In this paper, the maximum and minimum methods are used for normalization, and the mathematical formula is:

$$\bar{x}_i = \frac{x_i - x_{\min}}{x_{\max} - x_{\min}} \tag{50}$$

$x_{\max}$  and  $x_{\min}$  are the maximum and minimum values in the data sequence, respectively.

At the same time, to ensure the randomness of the data, the order of the training data should be disturbed to avoid learning the sample data with fixed rules; noise may also exist in the training data. After the order is settled, the noise will be mixed into the standard data to reduce the negative impact of noise data [21,24,27].

### 4.3 FFRLS-EKF joint estimation of SOC

In the derivation process of the EKF algorithm, the nonlinear system is expanded by Taylor, the high-order terms are omitted, and only the first-order terms are retained so that the nonlinear system is approximately expressed by the linear system formula such that the battery system meets the EKF algorithm. However, it is found through experiments that EKF still exhibits substantial error when

estimating battery SOC, which is not suitable for application in engineering practice. In actual working conditions of the battery, the working state of the battery is changeable, especially at the end of discharge, the battery is not in the voltage plateau period, and the voltage drops faster. At this time, the chemical reaction environment inside the battery changes, the concentration polarization becomes larger, the reaction occurrence is slow, and the complexity of the reaction increases. If the approximate linear equation continues to be used, a larger error will result. Many scholars have adopted various optimization methods to improve the accuracy of the EKF algorithm. Some scholars use online parameter identification methods to improve the accuracy and real-time performance of estimating the required parameters[32].

When the EKF adopts online parameter identification, the estimation accuracy is improved to a certain extent, but there are still errors because FFRLS estimation parameters require specific conditions, and frequent excitation is required to generate a better identification effect. If the current approaches 0 within a short time, the parameters are easily affected by voltage; at the same time, FFRLS also has specific requirements for the estimated frequency because of the internal resistance of the parameter that the system needs to identify as changing slowly with respect to the SOC. If the calculated frequency is too fast, a large error will occur and increase the operational burden; FFRLS also produces a certain error when using the FFRLS algorithm. At the same time, the choice of the forgetting factor in the FFRLS algorithm will also affect the accuracy of parameter identification. If the value is large, the result will be unstable, and if the value is small, convergence becomes more difficult. Therefore, the parameter identification results of FFRLS can improve the accuracy of EKF, but there are still errors and the need for continued optimization[13,14,19,32].

The BP neural network is a relatively mature data training method. It provides the network with sufficient offline data, sets appropriate training parameters, and continuously adjusts the weights through the error between the output and expected results to form a perfect neural network. In this paper, a neural network is used to compensate for the mistake of EKF estimation. The parameters obtained in the iterative process of EKF are used as training data, and the appropriate activation function and training parameters are selected for training. The final output includes the EKF value and the SOC value obtained from the experiment. Adding the production of the neural network to the estimated value of EKF can obtain a more accurate SOC value[27].

The use of the EKF and FFRLS methods can ensure the real-time performance of SOC estimation and the timely updating of various parameters of SOC estimation. Using FFRLS and BP neural networks can ensure the robustness of SOC estimation and overcome the influence of the external environment on SOC estimation. Finally, a high-precision SOC is obtained[13,20].

#### *4.4 FFRLS-EKF-BPNN joint estimation steps*

The first step is to initialize the algorithm parameters, as described in Chapter 3 and Chapter 4 (4.1 and 4.2), to initialize the parameters of the FFRLS, EKF and BP neural network.

The second step is to train the BP neural network to build a four-input, one-output four-layer neural network with two hidden layers. The first hidden layer includes 10 neurons, and the second

hidden layer has 10 neurons The maximum number of iterations is 5000, and the expected value is 0.009. The training data are the charge and discharge data of the lithium iron phosphate battery under the constant current condition with 0.5C current, the charge and discharge data under the NEDC condition, and the charge and discharge data under the UDDS condition. In the EKF iteration process, innovation  $e$ , Kalman gain  $K$ , state vector difference  $\hat{x}_k - \hat{x}_k^-$ , and terminal voltage  $U_t$  estimated by the EKF are obtained. Let  $SOC_{实验} - SOC_{EKF}$  be the output of the neural network. Training uses 80% of the data, with 20% as the test sample. When the error is less than the expected value, neural network training is completed[38,39].

The third step is to use FFRLS to perform online parameter identification and incorporate current, terminal voltage and other measured values to be brought into the algorithm for calculation to obtain various parameters  $R_0, R_s, R_p, C_s, C_p$  in the equivalent circuit model at this moment.

In the fourth step, the EKF algorithm uses the equivalent circuit model parameters obtained in the third step and simultaneously uses the terminal voltage, current and other observations to perform EKF iterative calculations to obtain the state vector difference  $\hat{x}_k - \hat{x}_k^-$ , algorithm gain  $K$ , and innovation  $e$  at time  $k$ . The estimated terminal voltage and other parameters are generated in the algorithm process of  $U_t$ , and  $SOC_{EKF}$ .

The fifth step is to take the four parameters obtained in the fourth step as the input vector, bring them into the BP neural network trained in the second step, and add the output result to the result of the EKF estimated SOC in the fourth step. The result of FFRLS-EKF-BP joint estimation of SOC is found according to  $SOC_{EKF+FFRLS} + SOC_{BP}$ . Figure 5 is the flow chart of the joint estimation[28,29,30].

## 5. EXPERIMENTAL RESULTS

### 5.1 Experimental equipment and objects

**Table 2.** Test object information

Battery type	voltage range	Rated capacity	Standard discharge current	Standard charging current	Operating temperature
Lithium iron phosphate	2.5 V-3.65 V	60AH	30A	30A	-20-50°C

**Table 3.** Experimental equipment information

Equipment	Model	Voltage range	Current range	Operating temperature
Battery test system	LANHE 5V100A	0-5 V	0.2-100A	-20-50°C
equipment		Temperature control range	Temperature accuracy	Constant temperature fluctuation
Temperate box		5-60°C	0.1°C	0.5°C

The experimental objects and experimental equipment are shown in Figure 6

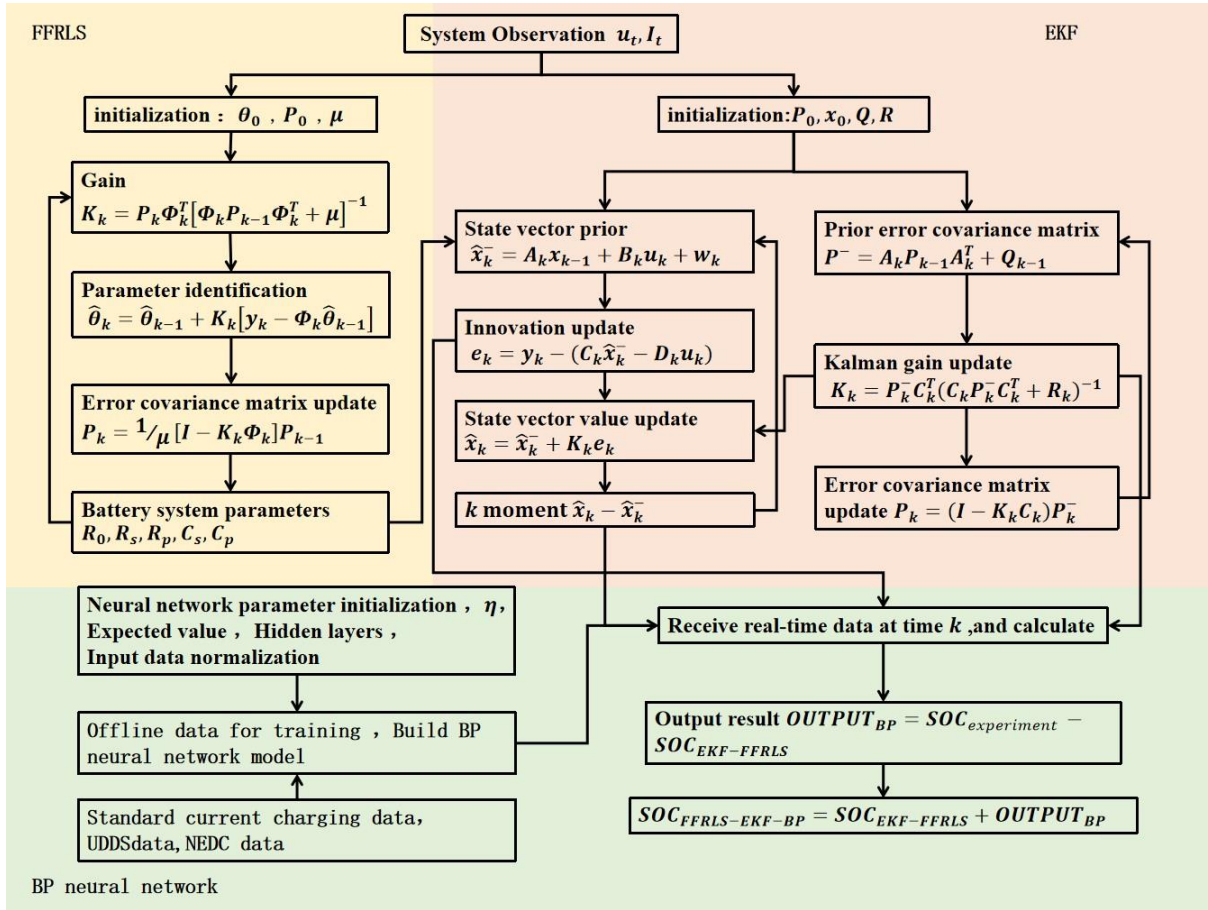


Figure 5. FFRLS-BPNN-EKF estimation process

To ensure that the test subjects adapted to the experimental environment before the experiment, put the battery was equilibrated for 24 hours in advance, and then use the battery test system was used to perform charge and discharge experiments in a constant temperature environment. All experiments were completed in a 25°C constant temperature environment[35]. The working condition utilized in the experiment is a specific dynamic working condition of the battery, as shown in Figure 7.

## 5.2 FFRLS-EKF-BPNN joint simulation results

### 5.2.1 BP neural network training

Experiments were performed on the battery under constant current charging and discharging conditions, UDDS operating conditions, and NEDC operating conditions, using EKF to estimate SOC under these conditions, and save the new information regarding EKF estimation process, Kalman gain, and a priori state of the system was saved. The value of the difference between the vector and the system vector in the posterior state, the estimated terminal voltage, and the abovementioned offline

data were collected to prepare for the training of the training neural network. Figure 8 shows the estimation of SOC under various working conditions using the EKF[34].



Figure 6. Experimental equipment and experimental objects

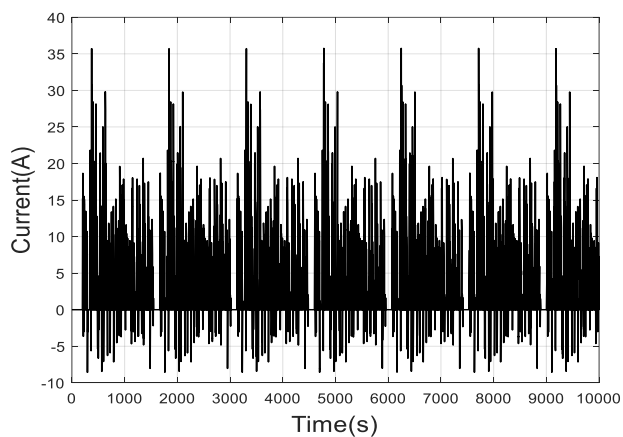


Figure 7. Simulation dynamic conditions

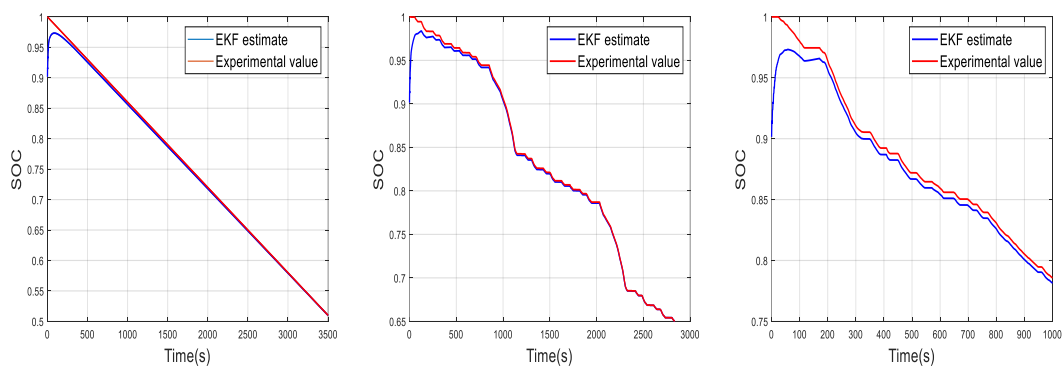


Figure 8. EFK estimated SOC diagram under three working conditions

Figure 9 depicts the training results when taking the obtained data as input, using 80% of the data for training and 20% of the data as testing data. The absolute coefficient of the neural network training result is 0.93. Because of the richer training data and reasonable training parameter values, the estimation results with smaller errors can be obtained. The maximum error is 0.02, and the BP neural network training is completed[27,29,30,33].

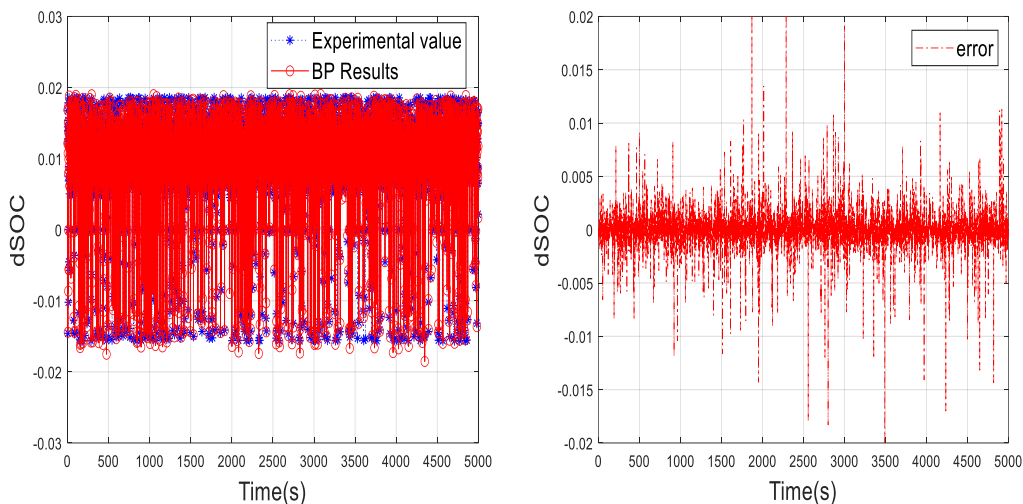
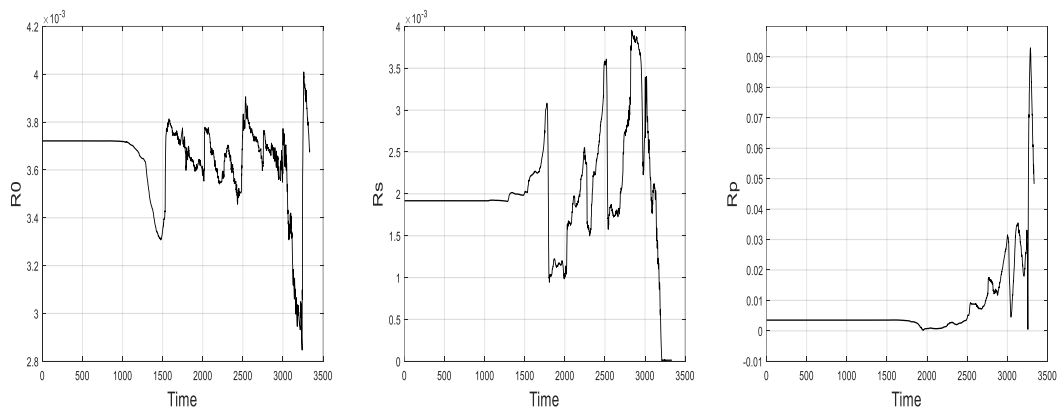
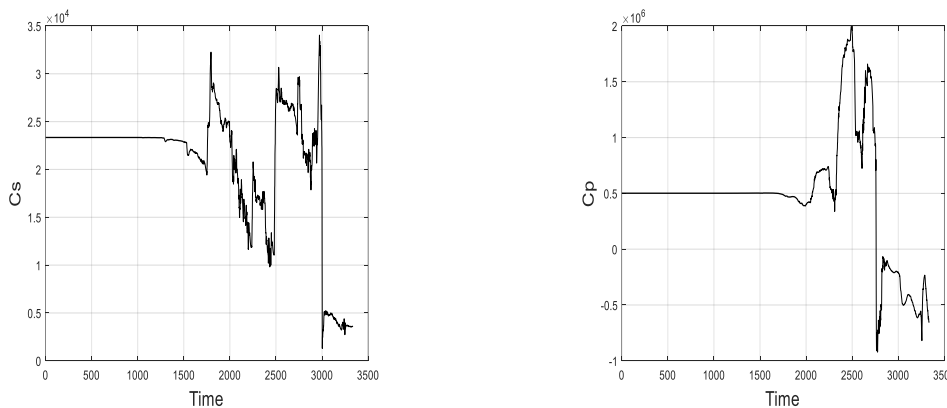


Figure 9. BP neural network training results

### 5.2.2 FFRLS-EKF-BPNN estimate SOC

The running algorithm first performs parameter identification, and then incorporates the parameter identification result into the EKF for SOC estimation. Figure10 shows the result of online parameter identification using the FFRLS algorithm[14,37].





**Figure 10.** Parameter identification result of FFRLS method

After the parameter identification is completed, the EKF algorithm is used to estimate the SOC. Figure 11 is a comparison diagram of the EKF and FFRLS-EKF algorithms. It can be clearly seen in the right figure that the estimation accuracy of the SOC estimation method using the online recognition algorithm is higher than that of the offline parameters [14,24]. This paper uses the estimation results of FFRLS-EKF for neural network training.

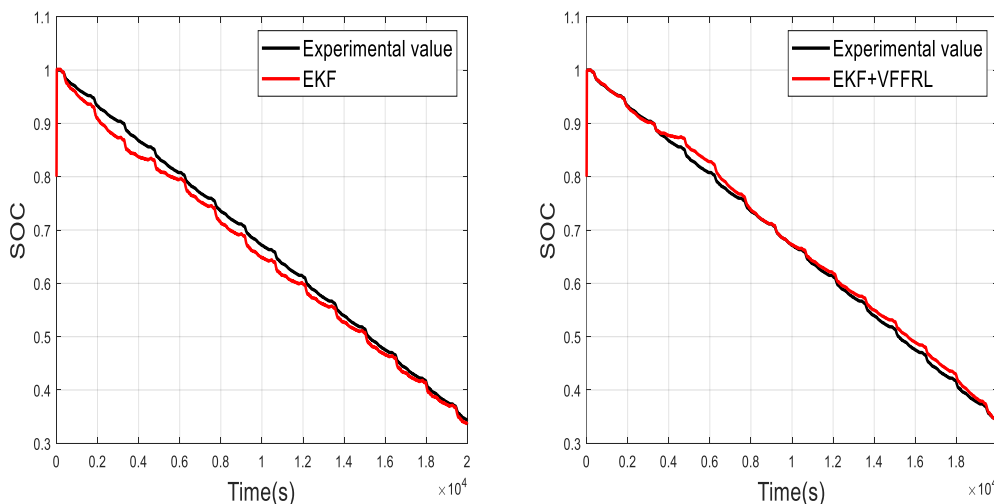


**Figure 11.** Estimation of SOC results by EKF and EKF-FFRLS methods

Afterwards, the BP neural network is used for error compensation. Figure 12 is the comparison between the predicted value and the experimental value. The difference between the prediction result of the neural network and the original value is small, the maximum error is 0.0055, and the average absolute error is 0.008 [27,29,34].

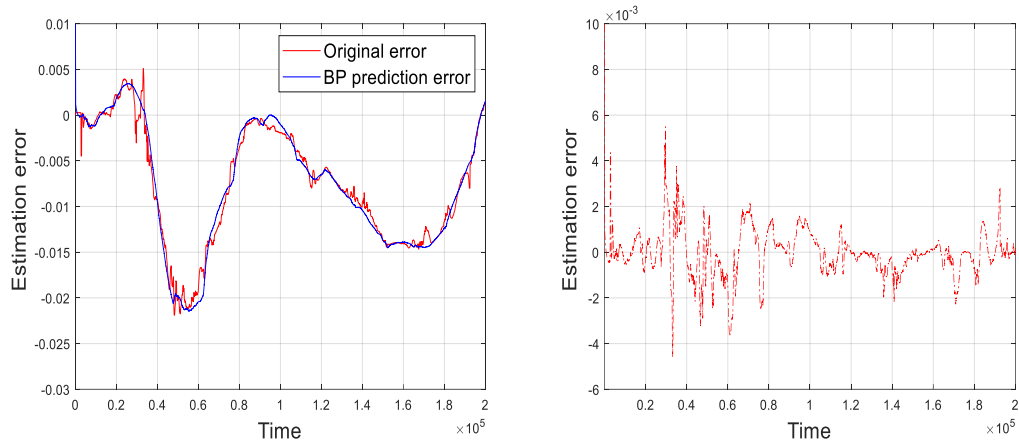


Figure 12. Neural network predicted value and error value

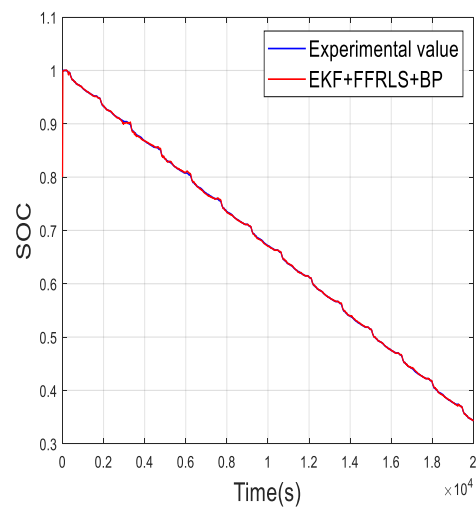


Figure 13. FFRLS-EKF-BPNN estimated value

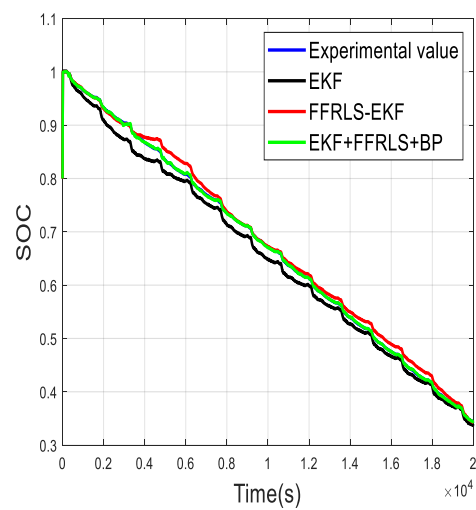


Figure 14. SOC values obtained by value four methods

**Table 4.** Error comparison

	Maximum absolute error	Mean absolute error	Root mean square
EKF	0.0356	0.0157	0.0176
FFRLS+EKF	0.0215	0.0081	0.0102
FFRLS+BP+EKF	0.0055	0.0008	0.001

**Table 5.** Error compared with other SOC estimation methods

<b>This study</b>	Maximum absolute error
EKF	0.0356
FFRLS+EKF	0.0215
FFRLS+BP+EKF	0.0055
<b>Other studies</b>	
Dual Extended Kalman Filter	0.02
UKF	0.02
GNL-AUKF	0.01
BPNN-UKF	0.035
ANN-EKF	0.028
Dual Neural Network	0.034
Improved RBFNN	0.03

Figure 13 shows the result of the FFRLS-EKF-BPNN method for SOC estimation. Figure 14 is a comparison of the results of several methods used in this article. Table 4 presents the error of several methods used in this article. Table 5 shows the errors of other research methods. The figure and table show that the FFRLS-EKF-BP method can effectively improve the SOC estimation and accuracy, which produces a better estimation result than original value. The maximum mean square error is 0.0055, and the root mean square error is 0.0001. Except for the initial value, the maximum absolute error of other parts can be controlled within 0.01. The figure and table show that the FFRLS-EKF-BP method can effectively improve the SOC estimation and accuracy, which yields a better estimation result than the original value. Due to the error compensation of the neural network method, the estimation accuracy and robustness of the system are increased, and the result is better than those of other estimation methods [25,26,32,35,36,37]. At the same time, there is no need to consider the influences of temperature, cycle life, or other parameter on the accuracy of the model, which can meet actual engineering needs [30,31,33,40].

**6. CONCLUSION**

(1) The use of the second-order RC network equivalent circuit model and the combined use of FFRLS-EKF can effectively improve the accuracy of SOC estimation, increase the real-time performance of battery model parameter updates, and overcome the impact of the external

environment on the battery system.

(2) Providing BPNN with sufficient data and appropriate training requirements can effectively compensate for the error of FFRLS-EKF, improve the accuracy of SOC estimation, and increase the robustness of the battery SOC estimation system.

## References

1. R. T. Doucette, MD McCulloch, *Applied Energy*, 88 (2011) 2315.
2. H. He, R. Xiong and J. Fan, *Energies*, 4 (2011) 582.
3. A. Fotouhi, D. J. Auger, K. Propp, S. Longo and Mark Wild, *Renewable and Sustainable Energy Reviews*, 56(2016)1008.
4. K. S. Ng, Y. F. Huang, C. S. Moo, Y. C. Hsieh, *International Telecommunications Energy Conference*, (2009)1.
5. Y. Zhang, W. Song, S. Lin and Z. Feng, *Journal of power sources*, 15(2014)1028.
6. W. Waag, C. Fleischer and D. U. Sauer, *Journal of Power Sources*, 258(2014)321.
7. Y. Gao, R. Huang and D. Qin, T. Wang, S. Ma, S. Qin, *int. J. Electrochem. Sci.*, 16 (2021) 210424.
8. C. Lin, B. Qiu and Q. Chen, *Automotive Engineering*, 28(2006)38.
9. J. Li, J. K. Barillas, C. Guenther and M. A. Danzer, *Journal of Power Sources*, 230 (2013) 244.
10. S. Yuan, H. Wu, X. Zhang and C. Yin, *IEEE Vehicle Power and Propulsion Conference*, (2013)1.
11. H. He, R. Xiong, X. Zhang, F. Sun and J. Fan, *IEEE Transactions on Vehicular Technology*, 60 (2011) 1461.
12. H. He, R. Xiong and H. Guo, *Applied Energy*, 89(2012)413.
13. F. Guo, G. Hu, S. Xiang, P. Zhou, R. Hong and N. Xiong, *Energy*, 178(2019)79.
14. C. Zhang, W. Allafi, Q. Dinh, P. Ascencio, J. Marco, *Energy*, 142(2018)678.
15. F. Sun, R. Xiong, *Journal of Power Sources*, 274(2015)582.
16. H. He, R. Xiong, H. Guo and S. Li, *Energy Conversion and Management*, 64(2012)113.
17. H. Rahimi-Eichi, F. Baronti and M. Chow, *IEEE Transactions on Industrial Electronics*, 61 (2013) 2053.
18. H. Rahimi-Eichi, F. Baronti and M. Chow, *IEEE International Symposium on Industrial Electronics*, (2012) 1336.
19. Y. Zhang, R. Xiong, H. He and W. Shen, *IEEE Transactions on Power Electronics*, 32 (2017) 4421.
20. C. Hu, B. D. Youn and J. Chung, *Applied Energy*, 92(2012)694.
21. M. Charkhgard, M. Farrokhi, *IEEE Transactions on Industrial Electronics*, 57(2010)4178.
22. Y. Wang, C. Zhang and Z. Chen, *Applied Energy*, 137(2015)427.
23. M. Mastali, J. Vazquez-Arenas, R. Fraser, M. Fowler, S. Afshar and M. Stevens, *Journal of Power sources*, 239 (2013) 294.
24. X. Guo, L. Kang, Y. Yao, Z. Huang and W. Li, *energies*, 9(2016)100.
25. R. Xiong, F. Sun and Z. Chen and H. He, *Applied Energy*, 113(2014)463.
26. X. Yan, Y. Guo and Y. Cui, Y. Wang and H. Deng, *First International Conference on Advanced Algorithms and Control Engineering*, 1087 (2018) 052027.
27. C. Dong, G. Wang, *IEEE International Conference on Mechatronics & Automation*, (2014) 2022.
28. C. Chang, Z. Liu and Y. Huang, *Computer Aided Drafting, Design and Manufacturing*, 24 (2014) 60.
29. B. Sun, L. Wang, *International Workshop on Intelligent Systems and Applications*, (2009)1.
30. B. Cheng, Z. Bai and B. Cao, *Energy Conversion and Management*, 48(2008)2788.
31. X. Dang, L. Yan, K. Xu, X. Wu, H. Jiang and H. Sun, *Electrochimica Acta*, 188(2016)356.
32. H. He, H. Qin, X. Sun and Y. Shui, *Energies*, 6(2013)5088.

33. B. Xia, D. Cui, Z. Sun, Z. Lao, R. Zhang, W. Wang, W. Sun, Y. Lai and M. Wang, *Energy*, 153 (2018) 694.
34. Y. Guo, Z. Zhao and L. Huang, *Energy Procedia*, 105(2017)4153.
35. V. Q. Dao, M. C. Dinh, C. S. Kim, M. Park, C. H. Doh, J. H. Bae, M. K. Lee, J. Liu and Z. Bai, *energies*, 14(2021)2634.
36. W. He, N. Williard, C. C. Chen and M. Pecht, *Electrical Power and Energy Systems*, 62(2014)783.
37. X. Dang, L. Yan, K. Xu, X. Wu, H. Jiang and H. Sun, *Electrochimica Acta*, 188(2016)356.
38. E. Chemali, P. J. Kollmeyer, M. Preindl and A. Emadi, *Journal of power sources*, 400 (2018) 242.
39. S. Tong, J. H. Lacap and J. W. Park, *Journal of Energy Storage*, 7 (2016) 236.
40. L. Kang, X. Zhao and J. Ma, *Applied Energy*, 121 (2014) 20.

© 2022 The Authors. Published by ESG ([www.electrochemsci.org](http://www.electrochemsci.org)). This article is an open access article distributed under the terms and conditions of the Creative Commons Attribution license (<http://creativecommons.org/licenses/by/4.0/>).